The Design of a Biaxial Micro Mirror

Xiaoping Zhang, Yahong Yao, Gaofeng Wang, Liji Huang and Naiqian Han
Intpax Inc., San Jose, CA 95134, USA, xzhang@intpax.com

ABSTRACT

A simplified design methodology for an electrostatic actuated biaxial micro optical mirror is developed. The relations among the pull-in angle, lift space, electrode size and applied voltage are derived. The analytical and FEM simulation results are compared. It is found that with a constant correction coefficient the results from the analytical formula match well to those by the FEM simulation. Consequently, the analytical guideline can be applied for a fast prototype design whereas the time-consuming FEM is only needed for the design verification. This design methodology has been successfully applied to a specific micro mirror design.

Keywords: micro mirror, MEMS, optical, thin film actuator, microstructure design.

1. INTRODUCTION

Micro optical mirror has many applications in the light steering devices such as photonic switches, scanners and digital projectors because of its small size and fast dynamics [1-3]. Previous researchers have focused on modeling, design and fabrication for one axis mirrors [4]. Recently, two or more axis micro mirrors have attracted extensive attentions because biaxial mirror allows a full 360° rotation at up to a certain tilt angle that can manipulate light in free space. Further, when forming a 3-D mirror array it dramatically reduces the device size [1]. However, the design methodology is not quite mature even though there are prototype biaxial mirror products in the market [5]. The design based on FEM requires complicated computation, resulting in a long design cycle, not even to mention the design optimization.

This paper provides a simplified analytical methodology working as the rule of thumb for designing a biaxial micro mirror (Fig. 1). With a novel structure possessing the capability of decoupling dynamics, an analytical model is established based on the rigid mirror plate assumption. Relations among the pull-in angle, lift space, electrode size and applied voltage are derived and simplification is achieved. Different from previous results [4], the performance index of the actuator is an explicit function of geometric parameters. This analytical methodology enables fast prototype design and optimization for this type of 2-D actuator. Since the results from the analytical approach are quite comparable to those from FEM simulation, it can be used for a fast simulation of initial design. This design methodology has been successfully applied to a specific 2-D micro mirror.

2. MIRROR DESIGN THEORY

2.1 The Governing Mechanical Equation and Decoupling Design

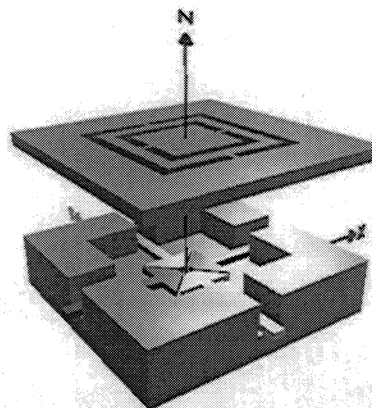

Figure 1: Micro mirror (four triangular type electrodes against mirror plate ground).

The biaxial mirror is a simplified robot (Fig. 1). The mirror plate is the end-effector. Its orientation is controlled by the balance between the electrostatic torque and the restoring torque from two elastic hinges. The hinges may be taken as revolute joints with springs attached on them. For simplification reason, it is assumed that the mirror plate is rigid, and the electrostatic force is taken as the external force acting on the mechanical system. Thus the mechanical domain is separated out and the mirror mechanism analysis can be approached using energy method, i.e. as a mechanical system, the mirror dynamics can be derived using Lagrangian formulation [6]:

$$\frac{d}{dt}\frac{\partial}{\partial \dot{q}_i}L(q,\dot{q}) - \frac{\partial}{\partial q_i}L(q,\dot{q}) = F_i \qquad 1 \le i \le n \tag{1}$$

where $L(q,\dot{q})=T(q,\dot{q})-U(q,\dot{q})$ with $T(q,\dot{q})$ as the kinetic energy and $U(q,\dot{q})$ as the potential energy. $T(q,\dot{q})$ can be calculated as [6],

$$T(q,\dot{q}) = \sum_{k=1}^{n}[(\vec{\vartheta}_k)^T m_k \vec{\vartheta}_k + (\varpi_k)^T D_k \varpi_k]/2 \tag{2}$$

with m_k as the mass of link k, $\vec{\vartheta}_k$ as the mass center velocity of link k about base frame origin, ϖ_k as the link k angular velocity about its mass center originated local frame, D_k as

the link k inertia tensor about its mass center originated local frame, where

$$D_k = \begin{bmatrix} \int_V (y^2+z^2)\rho dV & -\int_V xy\rho dV & -\int_V xz\rho dV \\ -\int_V xy\rho dV & \int_V (x^2+z^2)\rho dV & -\int_V yz\rho dV \\ -\int_V xz\rho dV & -\int_V yz\rho dV & \int_V (x^2+y^2)\rho dV \end{bmatrix}$$

For two-axis mirror with mirror plate of length a, width b, thickness h, and density ρ, a symmetric design (inertial is symmetric to geometric principal axis) will diagonalize the inertia matrix D_k to $D_k = [D_{xx}\ 0;\ 0\ D_{yy}]$, with inertia along the x-axis $D_{xx} = \rho hab^3/12$ and the inertia along the y-axis $D_{yy} = \rho hba^3/12$. Also, the hinge spring constants can be calculated as $k_1 = 4GI_p / l_1$ and $k_2 = 4GI_p / l_2$ with $I_p = t^3 w\,[1/3 - 0.21\ t/w\ (1-t^4/12/w^4)]$, where G is the hinge material shear modulus, t is the hinge thickness, w is the hinge width, l_1 and l_2 are the hinge lengths.

Define $q = [\theta_1\ \theta_2]$ then kinetic energy is $T = 0.5\dot{q}^T D_k \dot{q}$ and potential energy is $V = 0.5 q^T K_k q$ where $K_k = [k_1\ 0;\ 0\ k_2]$. Applying Lagrange equation leads to

$$\begin{cases} D_{xx}\ddot{\theta}_1 + k_1\theta_1 = \tau_1 \\ D_{yy}\ddot{\theta}_2 + k_2\theta_2 = \tau_2 \end{cases} \quad (3)$$

Thus the natural modes induced by the mirror hinges are

$$f_1 = (k_1/D_{xx})^{0.5}/(2\pi),\ \ f_2 = (k_2/D_{yy})^{0.5}/(2\pi) \quad \text{(Hz)} \quad (4)$$

2.2 The Rotation under Electrostatic Force

Before we go further to calculate the torques in Eq. (3), the shape of electrodes has to be defined. For symmetry and simplification purpose we select the triangular shape as shown in Fig.2.

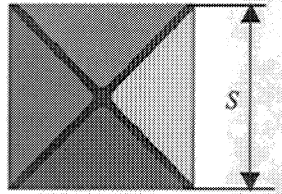

Figure 2: Bottom Electrodes.

Then the torque τ_1 around hinge 1 may be calculated as [4],

$$\tau_1 = \int_0^{S_a/2} x \int_{-x}^{x} \varepsilon V_1^2 / 2 / (g - xtg\theta_1 + ytg\theta_2)^2 dydx \quad (5)$$

where g is the gap between bottom electrodes and mirror plate, ε is the air media dielectric constant, $S_a = S$ is the electrode edge size (Fig. 2) in x direction, V_1 is the applied voltage at electrode 1, θ_1 and θ_2 are the rotation angles around two hinges, respectively.

Since the symmetric design provides decoupled actuation, the following analysis will only focus on the rotation around one hinge. The subscript will be removed in the following analysis. Also, the term $ytg\theta_2$ will be removed from Eq. (5) since it dose not have much influence on the integral value. Substitute Eq. (5) into Eq. (3), the steady state solution gives:

$$V^2 = (4GI_p / l / \varepsilon)\theta tg^3\theta / [g^2/(g - Stg\theta/2) + 2g\ln(g - Stg\theta/2) + Stg\theta/2 - g - 2g\ln g] \quad (6)$$

The maximum rotation angle is reached at the peak point where pull-in takes place, which can be calculated through investigating $dV^2/d\theta = 0$, as

$$[3u+8g\ln(g-u)-(4g+8g\ln g)](g-u)^2+(2gu+4g^2)(g-u)-g^2u = 0 \quad (7)$$

where $u = S\theta/2$.

It is interesting that the relation between u and g in Eq. (7) is not dependent on other design parameters. In order to show straightforward relationship between them, additional simplification has to be made. The u v.s. g is found to be linear as shown in Fig.3.

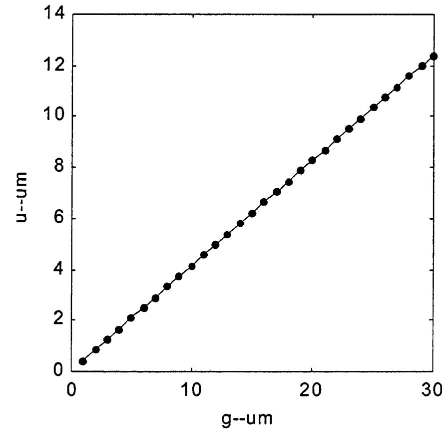

Figure 3: u vs. g is linear.

And more precisely, the ratio (u/g = 0.41) can be obtained from the above graph, i.e.,

$$\theta_{max} = 0.82\ g/S \quad (8)$$

Thus the first design rule can be determined as part of the theoretical design guidance:

Rule of thumb I – maximum rotation angle is 82% of the ratio of gap g to electrode size S

Substitue Eq. (8) into Eq. (6), for small rotation angle, it results in,

$$V^2 \approx 80\ GI_p\ \theta^4 / (\varepsilon l g) \quad (9)$$

where $I_p = t^3w/3$ for square cross section hinge, i.e., $t = w$ case. This results in the second design rule:

Rule of thumb II – Voltage is depending on the hinge

In order to lower down the applied voltage, we prefer slender hinges and a larger spacer (implying a larger mirror plate according to Rule of thumb I). However, a larger

mirror plate will result in lower natural mode and a larger device size. Also, large lift space g will lose the privilege of using air squeeze film damping effect, resulting in too much oscillation in the dynamic response results.

2.3 Other Design Considerations

After the interaction between electronic domain and mechanical domain being carefully checked in previous section and rule of thumbs formed, other design issues have to be considered. The following discusses the mechanical strength of hinges and fabrication processes.

2.3.1 Mechanical Strength

The most significant stress on the hinge is the hinge cross section shear stress:

$$\tau = 4GI_p\theta_{\max} / (\beta lt^3) \qquad (10)$$

For a square cross section hinge, $t = w$, Eq. (10) reduces to $\tau = 4Gw\theta_{\max} / (3\beta l)$ where $t \times w \times l$ is the hinge dimension, $\beta = 0.208$. The weight induced bending stress σ is negligible:

$$\sigma \approx 3\rho a^2 bh / (2tw^2) \qquad \text{(for } t = w \text{ case)} \qquad (11)$$

2.3.2 Geometric Constrains

$g > S\theta_{max}$. (Maximum rotation angle is limited by the gap and electrodes size.)
$l < 250$ μm. (Yield and other specs requires that pitch = 1mm, thus limit the device size and the hinge size.)

2.3.3 Fabrication

Design should take considerations of the constraint from fabrication steps. The above device is fabricated by a simple process with only three masks. Firstly, recess is made on the Si wafer by reactive ion etch (RIE) (1st mask). The depth of the recess defines the gap between mirror plate and the electrode. Then metal films Cr/Au is deposited and patterned (2nd mask). Electrodes stay at the bottom of the trench. Metal patterns on the wafer surface are for wafer bonding purpose which will be performed later. The mirror plate is made on a silicon on insulator (SOI) wafer (3rd mask) of which device layer thickness defines mirror plate thickness. Again dry etching is used to pattern the mirror plate and etching stops on the oxide. Then the SOI wafer is flipped over and bonded with the electrode wafer by Si-Au eutectic bonding. The handle Si is removed by RIE or wet etching. Finally, the oxide is stripped off by hydrofluoric acid. This simple process flow ensures a reasonable gap between mirror plate and electrodes. By this method, the mirror plate and the hinge maintain the same thickness.

3. A MIRROR DESIGN PRACTICE

Suppose the 2-D mirror design objective is to achieve a tilting angle of 0 ~ 1.7° for each axis when applying a voltage of 0 ~ 200V, respectively. Then the design procedure is:

Step 1. Design g and S as well as hinge size t, w and l

Combing Eqs. (8) and (9), and assume square cross section hinge, i.e. $t = w$, to get

$$S\,l / w^4 = 22G\theta_{\max}^3 / (\varepsilon V^2) \qquad (12)$$

$$g = 1.22\, S\, \theta_{\max} \qquad (13)$$

Set $\theta_{\max} = 1.7° = 0.03$ rad, and set $V = 200$ V as desired, the S, g, l and w relation are plotted in Fig. 4 and Fig. 5.

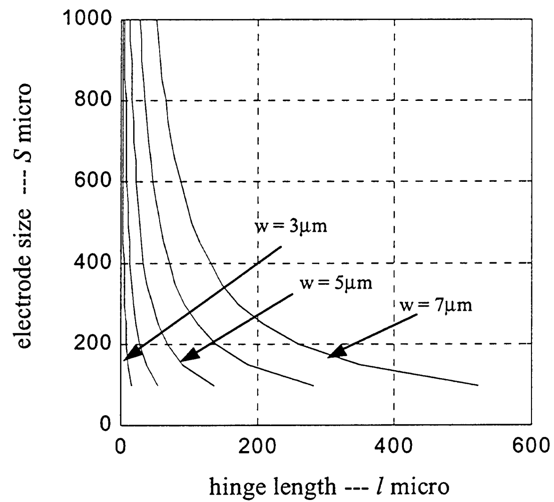

Figure 4: S, l, w relation for θ=1.7° @V=200V.

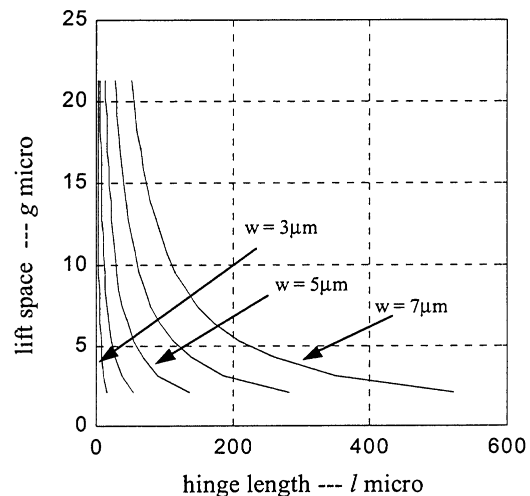

Figure 5: g, l, w relation for θ=1.7° @V=200V.

From Figs. 4 and 5, design parameters *l*, *g*, *S* and *w* may be determined by proper selection of parameter values. For a certain hinge width, Fig. 4 shows that the hinge length *l* should be large so that the electrode size *S* could be smaller, resulting in a large rotating clearance ($g > S\ \theta_{max}$) therefore a larger θ_{max}. However, from Fig. 5 the lift space *g* has a better tolerance to process variation if hinge length *l* gets smaller. On the other hand, the gap *g* should not be too large and too small so that the air damping can be properly equipped to achieve high dynamic performance. With these considerations in mind, it is seen that an appropriate parameter set can be chosen as: w = 5 μm, and l = 40 μm (this implies that hinge height t = 5μm and the mirror thickness h = 5 μm also), then the electrodes edge length S = 350 μm and the lift space g = 7.5 μm.

Step 2. Check natural mode and stress

Based on Eq. (4), the natural frequency can be investigated by setting $h = t$,

$$f_1=2/\pi/(Gwt^2/\rho\ lab^3)^{0.5} \quad \text{(Hz)} \qquad (14)$$

It is calculated as 47KHz by substituting the obtained design parameters in step 1. Also, according to Eqs. (10) and (11), the shear stress can be calculated as 0.9 GPa and bending stress is only 6.4 KPa, much less than the material yield strength. It is also easy to verify that the geometry constraints (see section 2.3.2) are also satisfied.

Step 3. FEM validation

After the analytical design phase, detailed simulation has to be executed for validation. Also, the assumption that the mirror is a rigid mass spring system will cause deviations from the analytical prediction. It is found that with a constant coefficient, the pull-in voltage predicted by analytical method matches very well with the FEM simulation result. For this case, V_{FEM} = V/1.75. The FEM simulation parameters and results are shown in Table 1. The pull-in characteristics are compared between analytical method and FEM at Fig. 6.

Table 1: FEM simulation parameter and results.

Parameter	Value	Parameter	Value
Lift space g	10 μm	Hinge width	5 μm
Electrode edge S	270 μm	Operation voltage	0 ~ 190 V
Mirror plate	300 × 300 × 5 μm^3	Operation angle	0 ~ 1.7°
Hinge length	40 μm	Maximum stress	0.39 GPa
Hinge thickness	5 μm	Natural modes	11.6KHz, 26.8KHz

4. CONCLUSION

A bi-axis optical micro mirror design is investigated and the rules of thumbs are formulated. The analytical formulae provide insights on the mirror design synthesis. The expressed guidance is concise and it can speed up the design process dramatically due to the reduced computing. Also, a design practice is performed using this methodology and the result is comparable to the FEM result. Other issues related to the fabrication process are also discussed in this paper. The design methodology can be extended to designs of a variety of micro devices.

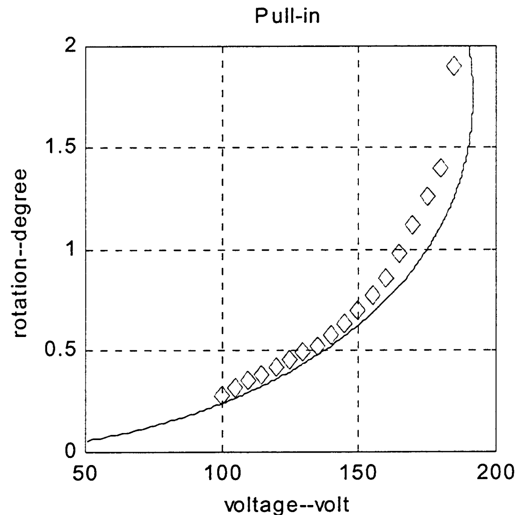

Figure 6: The mirror pull-in characteristics. (diamond dot: FEM result; solid: analytical result.)

REFERENCES

[1] P. B. Chu, S. S. Lee, S. Park, M. J. Tsai, I. Brener, D. Peale, R. Doran and C. Pu, "MOEMS – Enabling Technologies for Large Optical Cross-Connects," Proceedings of SPIE: MOEMS and Miniaturized Systems II, Vol. 4561, pp. 55-65, 2001.

[2] V. A. Aksyuk, F. Pardo, C. A. Bolle, S. Arney, C. R. Giles and D. J. Bishop, "Lucent Microstar Micromirror Array Technology for Large Optical Crossconnects," Proceedings of SPIE, MOEMS and Miniaturized Systems, Vol. 4178, pp. 320-324, 2000.

[3] H. Toshiyoshi and H. Fujifa, "An Electrostatically Operated Torsion Mirror for Optical Switching Device," Transducers '95, Eursosensors IX, 68-B1.

[4] X. M. Zhang, F. S. Chau, C. Quan and A. Q. Liu, "Modeling of the optical torsion micromirror," SPIE Conference on Photonics Technology into the 21st Century: Semiconductors, Microstructures, and Nanostructures, Singapore, pp. 109-116, SPIE Vol. 3899, 1999.

[5] V. R. Dhuler, M. Walters, R. Mahadevan, A. B. Cowen and K. W. Markus, "A Novel Two Axis Actuator for High Speed Large Angular Rotation," Transducers '97, International Conference on Solid-State Sensors and Actuators, Chicago, pp. 327-330, 1997.

[6] R. J. Schilling, "Fundamentals of Robotics – Analysis and Control," Prentice Hall, 1990.